

# Structural Basis of Plasticity in T Cell Receptor Recognition of a Self Peptide–MHC Antigen

K. Christopher Garcia,\* Massimo Degano,\* Larry R. Pease, Mingdong Huang, Per A. Peterson, Luc Teyton, Ian A. Wilson†

The T cell receptor (TCR) inherently has dual specificity. T cells must recognize self-antigens in the thymus during maturation and then discriminate between foreign pathogens in the periphery. A molecular basis for this cross-reactivity is elucidated by the crystal structure of the alloreactive 2C TCR bound to self peptide–major histocompatibility complex (pMHC) antigen H-2K<sup>b</sup>–dEV8 refined against anisotropic 3.0 angstrom resolution x-ray data. The interface between peptide and TCR exhibits extremely poor shape complementarity, and the TCR  $\beta$  chain complementarity-determining region 3 (CDR3) has minimal interaction with the dEV8 peptide. Large conformational changes in three of the TCR CDR loops are induced upon binding, providing a mechanism of structural plasticity to accommodate a variety of different peptide antigens. Extensive TCR interaction with the pMHC  $\alpha$  helices suggests a generalized orientation that is mediated by the V $\alpha$  domain of the TCR and rationalizes how TCRs can effectively “scan” different peptides bound within a large, low-affinity MHC structural framework for those that provide the slight additional kinetic stabilization required for signaling.

The phenomenon of MHC restriction is the basis of the cell-mediated immune response to foreign pathogens (1). The central molecular event governing this process is the engagement of the clonotypic  $\alpha\beta$  TCR by particular MHC class I or class II molecules in association with processed peptides (2). Upon engagement of the pMHC, a proliferative signal is transduced into the T cell by subsequent activation of the nonclonotypic members of the TCR signaling complex: CD8 (class I) or CD4 (class II), and CD3  $\gamma$ ,  $\delta$ ,  $\epsilon$ , and  $\zeta$  (3, 4).

It has become clear that a structural plasticity, or flexibility, in recognition of pMHC (5, 6) and a biological plasticity in response to ligand (3, 4, 7–9) are essential properties for the survival and function of T cells. Thymic development of T cells depends on weak interactions with self pMHC ligands (10). T cells selected for maturation then exhibit high frequencies of alloreactivity, or cross-reactivity, against both self and foreign pMHC complexes in the periphery (11).

This TCR cross-reactivity can manifest itself in a range of different biological outcomes, depending on the pMHC ligand (5–8), and includes agonist and antagonist effects (8), which have been correlated to the half-life of the TCR–pMHC complex and co-receptor association (12). An important question is whether there are structural properties unique to the TCR–pMHC interface that facilitate this broadened specificity.

T cell receptor structure determinations have illuminated similarities and differences with antibodies and how the TCR may be particularly suited to bind pMHC (13–16). The orientation of the TCR to the pMHC has been determined for two TCR–pMHC complexes (15, 16), one of which represents a refined structure at 2.6 Å (16). The overall topology of these complexes could be reconciled with earlier predictions inferred from biological data (17–19).

We have focused our efforts on the murine 2C TCR system (20, 21), which is the only  $\alpha\beta$  TCR for which distinct self (H-2K<sup>b</sup>–dEV8) (6) and foreign [H-2K<sup>b</sup>–dEV8 (6) and H-2L<sup>d</sup>–p2Ca (22)] ligands have been defined (23). Thymocytes of 2C transgenic mice are positively selected in the presence of H-2K<sup>b</sup> and negatively selected in the presence of the allo-ligands H-2K<sup>b</sup> (a naturally occurring, two-amino acid mutant of H-2K<sup>b</sup>) or H-2L<sup>d</sup> (21). dEV8 is a murine self-peptide, derived from intracellular processing of the murine mitochondrial respiratory protein complex (MLRQ), that was eluted from H-2K<sup>b</sup>- and H-2K<sup>b</sup>-bearing cells (6). When bound to H-2K<sup>b</sup>,

dEV8 is a weak agonist for the 2C cytotoxic T cell but a strong agonist for the 2C allo-ligand H-2K<sup>b</sup>. Therefore, dEV8 may be one of a number of peptides bound to H-2K<sup>b</sup> that is capable of selecting 2C thymocytes (6). A crystal structure of 2C in complex with H-2K<sup>b</sup>–dEV8 can allow us to explain how just two amino acid changes are sufficient to convert H-2K<sup>b</sup> into an alloreactive ligand (21).

We report here the refined crystal structure of the mouse 2C TCR in complex with mouse MHC class I H-2K<sup>b</sup> bound to the self-peptide dEV8 (EQYKFYSV) (24). We also briefly describe the 2.3 Å structure of H-2K<sup>b</sup>–dEV8, which, along with the unliganded 2.5 Å structure of the 2C TCR (15), allows us to assess whether there are structural alterations in either the TCR or pMHC upon complexation. We can now more clearly explain the degenerate specificity of TCR–pMHC interaction in terms of a structural plasticity in the TCR–pMHC interface. The ability to alter the shape of the TCR combining site through deformation of the peptide-contacting complementarity-determining region (CDR) loops and their side chain orientations, along with large unfilled spaces in the interface, permits useful accommodation of different ligands. This in turn gives rise to the biological and functional plasticity that is based on varying affinities and stabilities observed in most TCR systems in the *in vivo* signal transduction events.

**Overall structure.** The 2C TCR and H-2K<sup>b</sup>–dEV8 were expressed and purified from *Drosophila melanogaster* cells and co-crystallized (23). The structure was determined by molecular replacement and refined with the use of multidomain real-space averaging and torsion angle dynamics (25) (Table 1). The diffraction of these crystals is markedly anisotropic along the *b*<sup>\*</sup> direction, thus limiting the effective resolution of the refined structure (maximum resolution along *a*<sup>\*</sup> and *c*<sup>\*</sup> is beyond 3.0 Å, but only ~4.2 Å along *b*<sup>\*</sup>). Despite the presence of this anisotropic decay, all of the domains of the two TCR–pMHC complexes in the asymmetric unit are ordered (26), with the highest quality electron density being in the TCR–pMHC interfaces. The relation of the two molecules in the asymmetric unit (27) does not support other crystallographically derived dimerization models for TCR–pMHC complexes (28).

The overall relative orientations of the TCR and pMHC in the refined 2C–H-2K<sup>b</sup>–dEV8 complex are identical to those derived from the original molecular replacement solution (15). The TCR crosses the pMHC in an approximate diagonal orientation, in which the TCR  $\alpha$  chain lies over the bound peptide NH<sub>2</sub>-terminal residues

K. C. Garcia, M. Degano, M. Huang, and I. A. Wilson are in the Department of Molecular Biology and the Skaggs Institute of Chemical Biology, The Scripps Research Institute, 10550 North Torrey Pines Road, La Jolla, CA 92037, USA. L. R. Pease is in the Department of Immunology, Mayo Clinic, Rochester, MN 55905, USA. P. A. Peterson is at the R. W. Johnson Pharmaceutical Research Institute–La Jolla, 3535 General Atomic Court, San Diego, CA 92121, USA. L. Teyton is in the Department of Immunology, The Scripps Research Institute, 10550 North Torrey Pines Road, La Jolla, CA 92037, USA.

\*These authors contributed equally to this work.

†To whom correspondence should be addressed. E-mail: wilson@scripps.edu

and the  $\beta$  chain covers the peptide COOH-terminal residues (Figs. 1 and 2). Given the steric limitations that the MHC helices place on the depth of the approach of the TCR to the bound peptide, the diagonal orientation allows for the deepest docking solution of the TCR CDRs onto the pMHC surface. The unusual noncanonical fold of the TCR  $C_{\alpha}$  domain (15) is confirmed in each of the two complexes.

**The TCR-pMHC interface.** About 1876 Å<sup>2</sup> of surface is buried in the 2C-K<sup>b</sup> interface, of which 900 Å<sup>2</sup> is contributed by the TCR and 976 Å<sup>2</sup> by the pMHC (25). Within the pMHC composite surface, about 222 Å<sup>2</sup>, or 23% of the total, constitutes the bound dEV8 peptide, and 754 Å<sup>2</sup> (77%) the buried surface from the MHC  $\alpha$  helices. The small fraction of surface contributed by the peptide is a reflection of its deeply buried location within K<sup>b</sup> molecules, which limits the amount of exposed surface area, as originally proposed in the H-2K<sup>b</sup>-VSV and H-2K<sup>b</sup>-SEV structures (29). In the A6-HLA-A2-Tax complex (16), the total buried surface area in the interface is similar (30), but the peptide fraction is greater (33%).

All of the 2C TCR CDRs contribute to the buried surface area in the interface (Fig. 1), contrary to the situation seen in the structure of the human A6 TCR in complex with HLA-A2-Tax (30), where  $\beta$  chain CDRs 1 and 2 make essentially no contributions (16). For 2C, slightly more surface is buried by the  $\alpha$  chain (470 Å<sup>2</sup>) than the  $\beta$  chain (430 Å<sup>2</sup>), but within each chain the distribution of buried surface area by the CDRs varies: CDR1 $_{\alpha}$ , 214 Å<sup>2</sup>; CDR2 $_{\alpha}$ , 110 Å<sup>2</sup>; CDR3 $_{\alpha}$ , 140 Å<sup>2</sup>; CDR1 $_{\beta}$ , 160 Å<sup>2</sup>; CDR2 $_{\beta}$ , 167 Å<sup>2</sup>; CDR3 $_{\beta}$ , 89 Å<sup>2</sup>; and HV4, 10 Å<sup>2</sup>. CDR3 $_{\beta}$  contributes the least buried surface of all the CDRs and is positioned over a largely empty pocket in the interface (Fig. 1). The overall contact surface is formed from 21 TCR, 16 MHC, and 5 peptide residues (Table 2).

**TCR contacts with the MHC helices.** Of the ~41 total intermolecular contacts between the TCR and pMHC, 27 are derived from CDR contacts with highly conserved MHC  $\alpha$ 1 and  $\alpha$ 2  $\alpha$ -helical residues (Table 2). CDRs 2 $_{\alpha}$  and 2 $_{\beta}$  lie directly on top of the  $\alpha$ 2 and  $\alpha$ 1 helices, respectively, and, therefore, interact exclusively with the MHC (Fig. 2). CDRs 1 $_{\alpha}$  and 1 $_{\beta}$  lie between the helices and are thus able to contact both peptide and MHC simultaneously. As originally speculated (15), the paucity of bulky side chains at the apices of CDRs 2 and 3 in both chains (Fig. 2A) allows the 2C TCR to approach the MHC heavy chain so as to maximize main chain van der Waals contacts and to position the two CDRs to "read-out" the contents of the

**Table 1.** Data collection and structure determination. Crystals of the 2C-H-2K<sup>b</sup>-dEV8 complex (23) are orthorhombic (P2<sub>1</sub>2<sub>1</sub>2) with two TCR-pMHC complexes in the asymmetric unit. An x-ray data set was collected on a MAR imaging plate at the Stanford Synchrotron Research Laboratory on a crystal cryopreserved (20% ethylene glycol) and flash-cooled in a gaseous nitrogen stream. X-ray diffraction data from this crystal extended beyond 2.8 Å in the  $a^*$  and  $c^*$  directions, but the overall data were truncated to 3.0 Å because of a marked anisotropy along  $b^*$ , as judged from Wilson plots. The average  $\langle I/\sigma(I) \rangle$  at 3.0 Å resolution for  $a^*$  and  $c^*$  are 5.0 and 3.3, respectively. Along  $b^*$  the average  $\langle I/\sigma(I) \rangle$  drops below 2.0 at 5.3 Å and below 1.0 at 4.5 Å resolution, although some measurable data extend to 3.6 Å. All of the measured intensities were used in the subsequent structure determination and refinement. The effective resolution, defined as the resolution at which the total number of collected unique reflections equals a 100% complete data set (25), is 3.2 Å when all reflections with  $F > 0$ , or 3.38 Å for  $F > 2\sigma(F)$  are considered. Data were integrated and reduced with the DENZO and SCALEPACK programs (25). Initial phase estimates were obtained by molecular replacement. Rotation and translation functions (15.0 to 4.0 Å) were calculated with AMoRe (25), with the coordinates of the unliganded 2C TCR [PDB code 1TCR (15)] and H-2K<sup>b</sup>-OVA [1VAC (49)]. The Patterson maps for rotation function calculations were generated from normalized structure factors to sharpen their features and partially correct for the anisotropy. Only one solution for the TCR (peak heights of 6.5 $\sigma$  and 8.2 $\sigma$  in the rotation and translation function maps, respectively) and one solution for the MHC molecule (4.9 $\sigma$  and 9.4 $\sigma$ ) were clear at this stage. A native Patterson map showed a 7 $\sigma$  peak at fractional coordinates (0.46, 0.33, 0.5), suggesting that a local twofold symmetry axis, parallel to a crystallographic axis, described the relation between the two molecules in the asymmetric unit. A partial translation function map, calculated after fixing the already-positioned TCR-pMHC complex and using the model in the same orientation for the three-dimensional search, was manually inspected for the existence of a peak related by this intermolecular cross vector to the original solution. A 6.5 $\sigma$  peak located at (0.97, 0.82, 0.87) met this requirement. The second complex in the asymmetric unit was located on the basis of this solution of the translation function. Five envelopes encompassing the variable portion and constant regions of the TCR, the  $\alpha$ 1 $\alpha$ 2 domain and peptide of K<sup>b</sup>, the  $\alpha$ 3 domain of K<sup>b</sup>, and  $\beta$ 2M were generated with MAMA (25), and the rotation and translation matrices relating the different domains were calculated and improved with an electron density correlation optimization algorithm (RAVE) (25). Phases were calculated from the model to 5.5 Å, refined through real-space averaging and solvent flattening with RAVE, and gradually extended to 3.0 Å in 40 cycles. Electron density maps calculated from the improved phases allowed unambiguous rebuilding of the regions that underwent structural changes and allowed the introduction of the correct dEV8 peptide sequence. The structure was refined with positional and torsion angle dynamics refinement (25), restraining the main chain and side chain atom positions of the model by means of harmonic force constants, by using the program X-PLOR 3.851 (25). The model was rebuilt with the program O (25), according to  $\sigma_A$ -weighted electron density maps (25), real-space averaged maps, and "shake" omit maps calculated after 10% of the model was omitted (25). Progress of the refinement was monitored by the decrease of  $R_{\text{free}}$  (25) calculated from 4% of the unique data (1435 reflections). The anisotropic diffraction was partially corrected by introduction of an overall anisotropic tensor ( $B_{11} = 14.6 \text{ Å}^2$ ,  $B_{22} = -11.0 \text{ Å}^2$ ,  $B_{33} = 14.9 \text{ Å}^2$ ), which increased the atomic displacement parameter array by 17 Å<sup>2</sup> (the relative  $B$  values before the correction were  $V_{\alpha} = 22 \text{ Å}^2$ ,  $V_{\beta} = 25 \text{ Å}^2$ ,  $C_{\alpha} = 38 \text{ Å}^2$ ,  $C_{\beta} = 26 \text{ Å}^2$ , K<sup>b</sup>-dEV8 = 24 Å<sup>2</sup>, and  $\beta$ 2M = 26 Å<sup>2</sup>). Refinement was begun with strict noncrystallographic symmetry constraints and later substituted by restraints to minimize  $R_{\text{free}}$ . A flat bulk solvent correction was applied. Individual isotropic temperature factors were refined, resulting in a similar decrease in the conventional and free  $R$  values (3.1% drop in  $R_{\text{free}}$  and 3.7% drop in  $R_{\text{cryst}}$  compared with a 0.4% drop in  $R_{\text{free}}$  and 1.0% drop in  $R_{\text{cryst}}$  when refining two  $B$  values per residue), and acceptable Ramachandran plots [calculated with PROCHECK (25)]. Three ordered water molecules were located in the interface based on  $3\sigma F_o - F_c$  residual electron density and added to the final model. The crystallization, data collection, and structure determination of H-2K<sup>b</sup>-dEV8 are described in (50).

	2C-H-2K <sup>b</sup> -dEV8	H-2K <sup>b</sup> -dEV8
<i>Data collection</i>		
Resolution range	25.0–3.0 Å	25.0–2.3 Å
Collected reflections	314,268	463,190
Unique reflections	37,960	24,222
Completeness (%) <sup>*</sup>	83.3, 70.1 (3.2–3.0 Å)	96.7, 95.7 (2.4–2.3 Å)
$\langle I/\sigma(I) \rangle$ <sup>†</sup>	9.2, 2.0	21.0, 7.1
$R_{\text{symm}}$ <sup>†</sup>	8.8, 33.0	7.1, 29.0
<i>Refinement statistics</i>		
Resolution range	25.0–3.0 Å	20.0–2.3 Å
Number of reflections ( $F > 0$ )	34,092	24,043
Completeness (%)	78.5, 68.6 (3.2–3.0 Å)	
$R_{\text{cryst}}$ <sup>†</sup>	0.221	0.213
$R_{\text{free}}$ <sup>†</sup>	0.322	0.289
<i>Rms deviations</i>		
Bonds	0.009 Å	0.011 Å
Angles	1.9°	1.6°
Dihedrals	29°	28.3°
Impropers	1.1°	0.8°
<i>Ramachandran plot</i>		
Favored (%)	73.2	89.4
Allowed (%)	25.5	9.7
Generous (%)	1.3	0.9
Unfavored (%)	0	0

<sup>\*</sup>Calculated for all data, and outer shells as indicated.

<sup>†</sup>Symbols:  $R_{\text{cryst}} = \sum |F_o| - |F_c| / \sum F_o$ , where  $F_o$  and  $F_c$  are the observed and calculated structure factors, respectively and the summation is extended over all unique reflections. For  $\langle I/\sigma(I) \rangle$ ,  $I$  is the measured intensity. For  $R_{\text{free}}$ , the sum is extended over a subset of reflections excluded from all stages of refinement.  $R_{\text{symm}} = \sum \sum |I_i - \langle I \rangle| / \sum I_i$ , where  $\langle I \rangle$  is the average of equivalent reflections, and the sums are extended over all measured observations for all unique reflections.

peptide binding groove. The predominant interaction of the TCR with the MHC helices in this complex, as also observed in the A6-HLA-A2-Tax complex (16), provides structural confirmation of long-standing hypotheses that the TCR repertoire must have evolved primarily with reactivity toward conserved features of the MHC heavy chain so that the most diverse portions of the receptor can discriminate among antigenic peptides (17–19).

A number of contacts (Table 2) at the periphery of the interface between the MHC helices and CDRs 1 and 2 appear to be between highly conserved residues and may play a key role in dictating (or steering) a generalized orientation. In particular, Ser<sup>27α</sup> of CDR1<sub>α</sub>, which hydrogen bonds to the conserved K<sup>b</sup> residue Glu<sup>58</sup> (Fig. 3A), and Ser<sup>51α</sup> of CDR2<sub>α</sub> [contacts Glu<sup>166</sup> (Fig. 3A)] are the most frequently occurring residues to occur in V<sub>α</sub> gene sequences at these positions (31). These interactions between conserved residues are consistent with recent data indicating a critical role for V<sub>α</sub> residues 27<sub>α</sub> and 51<sub>α</sub> in the restriction of particular murine TCRs (V<sub>α</sub>3.1 and V<sub>α</sub>3.2) for MHC class I versus class II (32). In class II MHC molecules, the approximate corresponding residues of the class I H-2K<sup>b</sup> Glu<sup>58</sup> and Glu<sup>166</sup> are different but still highly conserved (33). Other potentially conserved contacts appear between α (Tyr<sup>31α</sup>) and β (His<sup>29β</sup>, Glu<sup>56β</sup>) chain residues to the MHC helices (Table 2).

Overall, the V<sub>α</sub> CDR1 and CDR2 contact residues appear to be more highly conserved not only within K<sup>b</sup>-restricted TCRs but also across other TCRs compared with the corresponding β chain contact residues. In the A6-HLA-A2-Tax crystal structure, the A6 TCR V<sub>α</sub> has a similar overall orientation as V<sub>α</sub> in our complex, but it has minimal contact between the β chain CDRs 1 and 2 and the pMHC. These similarities and differences would strongly infer that it is the α chain that dictates the orientation of that complex (discussed below).

A conserved framework for TCR binding to the MHC helices, or a generalized orientation, would enhance the flexibility in pMHC recognition by providing a scaffold in which the centrally located peptide can be finely sampled by the TCR (18). A large, conserved buried surface of relatively low affinity would facilitate short-lived complex formation by the TCR and MHC and subsequent “scanning” of the peptide (34).

A naturally occurring mutant of H-2K<sup>b</sup>, termed H-2K<sup>bm3</sup> (Asp<sup>77</sup> to Ser, Lys<sup>89</sup> to Ala), is an alloreactive ligand for, and negatively selects, the 2C TCR (21). When bound to dEV8, H-2K<sup>bm3</sup> generates a strong 2C cytotoxic T cell response (6). Of the two mutations in H-2K<sup>bm3</sup>, Asp<sup>77</sup> to Ser has

been identified as the one that causes the alloreactive response (21). In the 2C-H-2K<sup>b</sup>-dEV8 structure, Asp<sup>77</sup> lies underneath CDR2<sub>β</sub> but does not contact 2C; instead, it forms a hydrogen bond to the main chain of the P8 peptide residue. Replacement of Asp<sup>77</sup> with Ser could disrupt this peptide contact and potentially alter the position of the peptide residues in contact with the TCR (especially Ser<sup>77</sup>) and also the conformation of the COOH-terminal region of the α1 helix, which is in contact with CDR2<sub>β</sub>. Additionally, removal of the Asp<sup>77</sup> negative charge would alter the electrostatics of this patch of pMHC surface, which is buried by the TCR (35). Hence, even though Asp<sup>77</sup> is not in direct contact with the TCR, its removal would clearly cause structural and electrostatic changes perceptible to 2C and lead to an alloreactive response.

**TCR contact with bound peptide.** The dEV8 peptide (EQYKFYSV) (24) runs from CDR1<sub>α</sub> to CDR1<sub>β</sub> diagonally across the TCR surface between CDRs 3<sub>α</sub> and 3<sub>β</sub> (Fig. 2B), which lie primarily within the peptide

binding groove between the α helices (Fig. 2D). The TCR interaction with the peptide is mediated directly and indirectly by hydrogen bonds to the functional groups of the upward-facing side chains (P1, P4, P6, and P7) from CDRs 1<sub>α</sub>, 1<sub>β</sub>, 3<sub>α</sub>, and 3<sub>β</sub>, which are in simultaneous contact with the α1 and α2 helices of the MHC (Figs. 1 and 2). The large hydrophobic central cavity between CDRs 3<sub>α</sub> and 3<sub>β</sub> remains unfilled, contrary to our previous expectations (15); CDR3<sub>β</sub> appears to have only a very limited interaction with the peptide at residue Tyr<sup>P6</sup> through a single contact with Gly<sup>97β</sup> (Fig. 3B). Thus, CDR3<sub>β</sub>, which has been implicated in playing a primary role in peptide recognition in other TCRs (16, 36), has negligible direct contact with the dEV8 peptide in our complex.

Overall, the interface between the TCR and pMHC exhibits poor shape complementarity (37), large empty spaces, and precarious peptide contacts, which is consistent with the weak affinity of this complex (dissociation constant, K<sub>D</sub>, of ~10<sup>-5</sup>M)

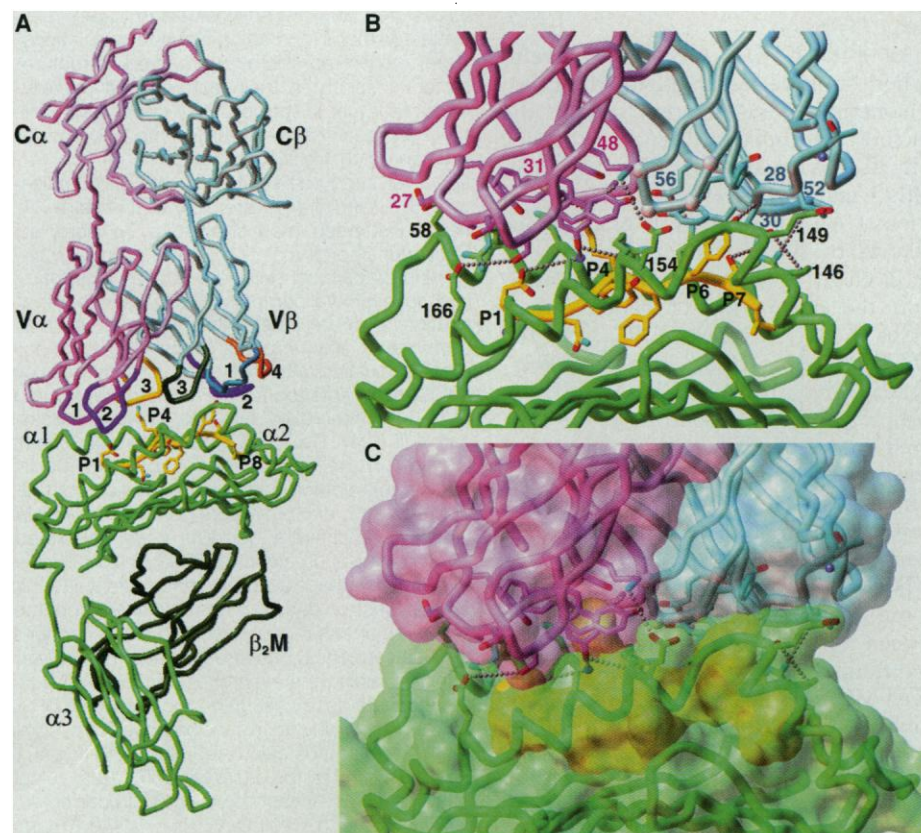


**Fig. 1.** Structure of the 2C-H-2K<sup>b</sup>-dEV8 complex. (A) Overall backbone structure of one entire TCR-pMHC complex [only one of the two complexes in the asymmetric unit of the crystal is shown (26)]. The TCR is on top (α chain pink, β chain light blue, CDR1<sub>α</sub> magenta, CDR2<sub>α</sub> purple, CDR3<sub>α</sub> yellow, CDR1<sub>β</sub> cyan, CDR2<sub>β</sub> navy blue, CDR3<sub>β</sub> green, HV4 orange). The pMHC is on the bottom (MHC heavy chain is green, β<sub>2</sub>-microglobulin (β<sub>2</sub>M) is dark green, peptide is yellow with side chains shown). (B) Close-up of the TCR-pMHC interface showing all side chains involved in intermolecular contacts, and hydrogen bonds are indicated. (C) Molecular surfaces of the interacting TCR, peptide, and MHC with backbones and side chains visible through the transparent surface. All figures were produced with Advanced Visual System (AVS) software, and surfaces were calculated with PQMS (25).



(23). The TCR interaction with the bound peptide antigen is through only the distal tips of the up-facing side chains, which are

required to be completely extended in order to reach the TCR, even when water molecules are used as a bridge (Fig. 3A and Table

2). There appears to be sufficient space between the peptide and TCR to accommodate a wide range of different peptide

**Fig. 2.** Combining sites and footprints of the 2C TCR and H-2K<sup>b</sup>-dEV8 molecules in the complex. **(A)** View into the combining site of the 2C TCR in the complex, shown without the pMHC. All residues of the TCR involved in contact with the pMHC are shown and labeled. Glycine residues are represented as white balls on the main chain ( $\alpha$  chain pink,  $\beta$  chain light blue, CDR1 <sub>$\alpha$</sub>  magenta, CDR2 <sub>$\alpha$</sub>  purple, CDR3 <sub>$\alpha$</sub>  light green, CDR1 <sub>$\beta$</sub>  red, CDR2 <sub>$\beta$</sub>  navy blue, CDR3 <sub>$\beta$</sub>  dark green, HV4 orange). **(B)** Same view into the 2C combining site, but with the interacting and nearby residues of the pMHC superimposed with the peptide in yellow and MHC helices in green. The view is from a perspective of the floor of the MHC peptide binding groove onto the TCR. The diagonal orientation and overall footprint is clear. **(C)** View into the pMHC combining site with peptide (yellow) and MHC (green). All pMHC residues involved in contact with the TCR are shown and labeled. Those MHC residues contacting the TCR  $\alpha$  chain are colored pink, and those contacting the TCR  $\beta$  chain are colored blue. **(D)** Same view into the pMHC combining site but with superimposition of the CDRs of the TCR onto the pMHC. It is clear in this representation that the CDR1s of both the  $\alpha$  and  $\beta$  chain as well as the CDRs 3 <sub>$\alpha$</sub>  and 3 <sub>$\beta$</sub>  are positioned along the central axis of the peptide binding groove. The NH<sub>2</sub>-terminal residues of the 2C V <sub>$\alpha$</sub>  domain appear (and are labeled "N") in the slicing plane, but do not interact directly with the pMHC, as in A6 (16).

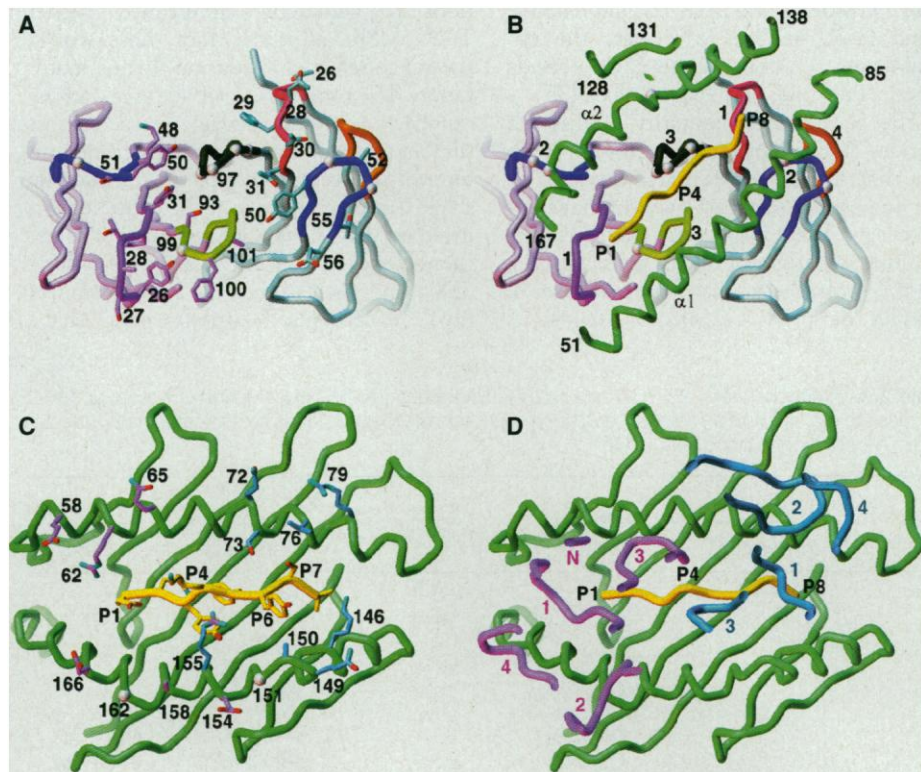
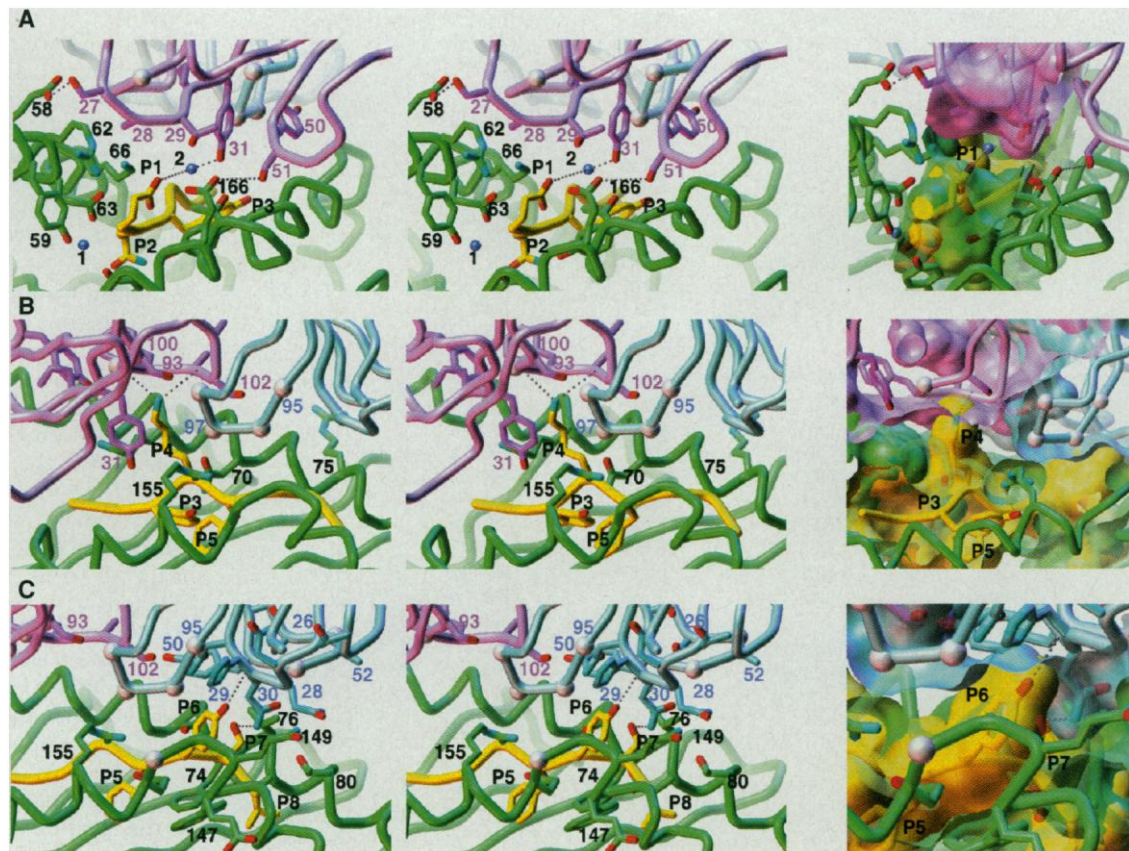


**Fig. 3.** Peptide-TCR interactions in the TCR-pMHC interface. In the left two panels, a stereo pair of the backbone and side chains of the TCR-pMHC interface are shown emphasizing the 2C interactions with the NH<sub>2</sub>-terminal P1 (A), middle P4 (B), and COOH-terminal P6-P7 (C) positions of the bound dEV8 peptide. In the companion panels to the far right, sliced molecular surfaces of the region shown in the left panels highlight the relatively poor complementarity of the peptide-TCR interaction. Large empty gaps in the TCR-pMHC interface are evident in the molecular surface representations. The TCR is shown in pink, the MHC in green, the peptide in yellow, and water molecules in blue.



residues, such as in the highly reactive synthetic peptide complex H-2K<sup>b</sup>-SIYR (SIYRYGYL) (24, 38), which contains different residues at the up-pointing P1, P4, and P7 positions, and in the 2C alloreactive ligand H-2L<sup>d</sup>-p2Ca (22), where the upward-facing positions of the p2Ca peptide contain Pro, Phe, and Asp residues (35).

The poor complementarity of this self peptide-TCR interface is consistent with data that suggest self peptides involved in thymic positive selection may not have exquisite specificity for a particular TCR (39) but instead cross-react with many TCRs. dEV8 is probably one of a degenerate set of peptides that positively select 2C (6), so its

precarious contacts with 2C are consistent with this promiscuous role.

The 2C-H-2K<sup>b</sup>-dEV8 complex also suggests the possibility of structural limitations to achieving significantly higher TCR-pMHC affinities than those within the range selected for during thymic maturation. The total buried surface area and the number of intermolecular interactions is similar to those found in high-affinity interfaces between proteins (40), but the shape complementarity in the center of this interface, between TCR and peptide, is extremely poor (37). In both 2C-H-2K<sup>b</sup>-dEV8 and the A6-HLA-A2-Tax complex (16), which also exhibits poor shape

complementarity (37), the peptide surface is effectively "held away" from the TCR combining site surface by the MHC  $\alpha$  helices, thus severely limiting the intimacy of this contact.

That the CDRs simultaneously contact MHC helical residues and peptide antigen bears on the issue of a bias in V-region subtypes toward particular antigens (41). In the 2C-K<sup>b</sup> structure, the bound peptide contacts both V (CDRs 1 and 3) and J (CDR3) segments of the V $\alpha$ , and V (CDR1) and D (CDR3) segments of the  $\beta$  chain (Table 2). Contacts of the V region with the bound peptide by both  $\alpha$  and  $\beta$  chains would skew the chain distribution toward sequences that can satisfy the dual requirements of recognition of both MHC helices (either conserved or polymorphic positions on the  $\alpha$ 1 and  $\alpha$ 2 helices) and peptide side chains (18, 42).

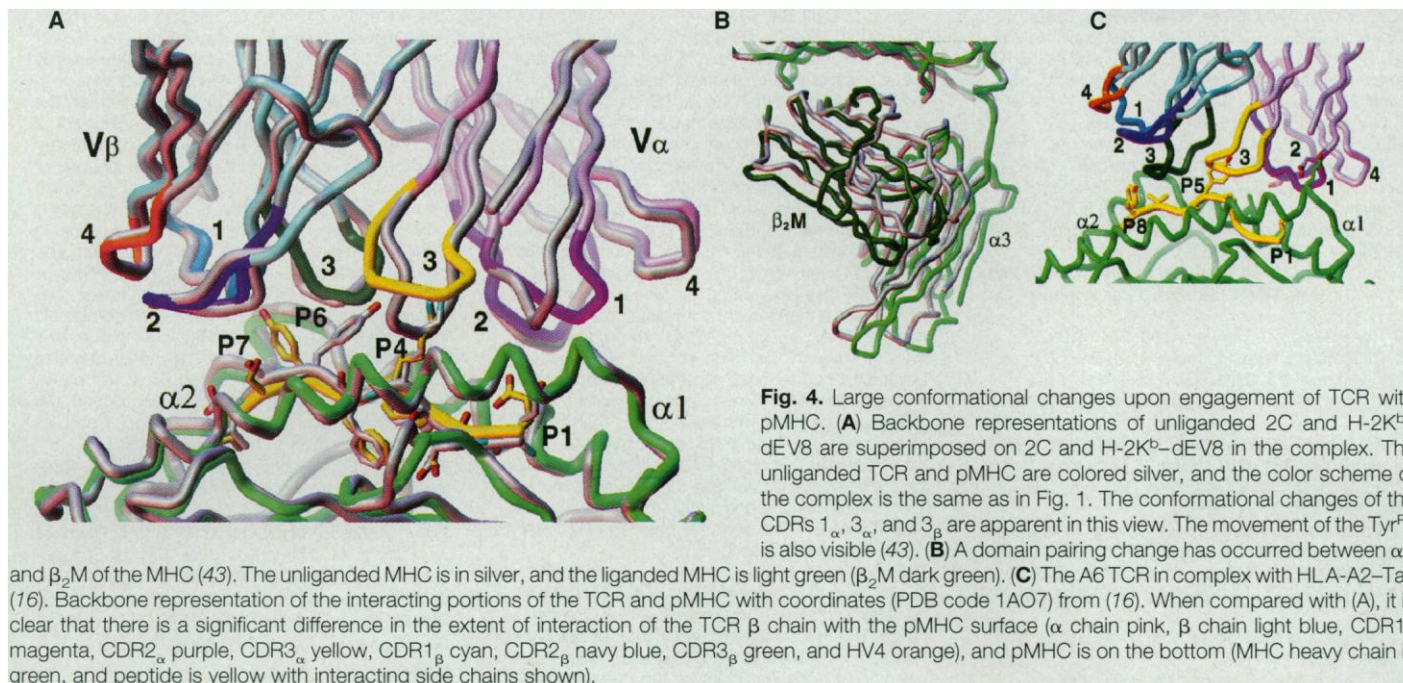
**Comparison of liganded and unliganded TCR and pMHC.** Comparison of the complex structure with the 2.5 Å unliganded 2C structure (15) and the 2.3 Å crystal structure of H-2K<sup>b</sup>-dEV8, which we only briefly describe here, has enabled us to identify large structural rearrangements that significantly affect the TCR-pMHC interaction. For 2C, the liganded and unliganded TCRs superimpose closely, showing no major domain rearrangements (26, 43). However, large accommodative movements have occurred in the three CDRs that are most intimately associated with peptide (Fig. 4A). The magnitude of these changes are large when compared with those seen so far in protein-antibody complexes (44). CDR1 $\alpha$  has undergone a hinge movement of ~4.2 Å between residues 25 $\alpha$  and 29 $\alpha$  to avoid collision with the MHC  $\alpha$ 1 helix (Fig. 4A). CDR3 $\alpha$  residues 99 $\alpha$  to 102 $\alpha$  [3.2 Å root mean square deviation (rmsd)] have undergone the largest conformational change of all the CDRs. In the unliganded 2C, this CDR has a type II'  $\beta$  turn, with Phe<sup>100 $\alpha$</sup>  protruding from the tip [see figure 8A in (15)]. In the complex, it is instead bent back by 6 Å so that the tip of the CDR interacts with the MHC  $\alpha$ 2 helix (Figs. 3B and 4A). The conformation of CDR3 $\beta$  is similar to that in the unliganded structure, with the exception of a small segmental shift (~1 to 2 Å) (Fig. 4A), which is consistent with its minimal direct contact with the pMHC surface (Table 2). The lack of movement of the other CDRs that primarily contact the MHC  $\alpha$  helices is consistent with their involvement in conserved interactions (Fig. 4A).

These large conformational adjustments to the pMHC (Fig. 4A), especially for the peptide-contacting CDRs, is an additional mechanism of enhancing the

**Table 2.** Contacts between 2C TCR and H-2K<sup>b</sup>-dEV8 peptide-MHC (51). Murine polymorphic MHC residues are marked with an asterisk, and gene segments of CDR3 residues are indicated. vdw, van der Waals; h-b, hydrogen bond; wat, water

CDR	TCR		Contact	pMHC	
	Residue	Atom		Residue	Atom
CDR1 $\alpha$	Tyr <sup>26<math>\alpha</math></sup>	O $\eta$	polar	Arg <sup>62</sup>	N $\eta$ 1
		C $\zeta$	vdw		C $\delta$ ,C $\gamma$
	Ser <sup>27<math>\alpha</math></sup>	O $\gamma$	h-b	Glu <sup>58</sup>	O $\epsilon$ 1
		C $\beta$	vdw		C $\delta$
		C=O	polar	Arg <sup>62</sup>	N $\eta$ 1
	Ala <sup>28<math>\alpha</math></sup>	C $\beta$	vdw	Arg <sup>62</sup>	C $\delta$
	Tyr <sup>31<math>\alpha</math></sup>	OH-wat	h-b	P1-Glu	O $\epsilon$ 1-wat
		OH-wat	polar	P2-Gln	C=O-wat
		C $\epsilon$	vdw	Arg <sup>155*</sup>	C $\delta$ ,C $\gamma$ ,N $\epsilon$
		O $\eta$	h-b	Arg <sup>155*</sup>	N $\epsilon$
CDR2 $\alpha$	Lys <sup>48<math>\alpha</math></sup>	N $\zeta$	h-b	Glu <sup>154</sup>	O $\epsilon$ 1
	Tyr <sup>50<math>\alpha</math></sup>	C $\delta$ ,C $\epsilon$	vdw	Arg <sup>155*</sup>	C $\beta$ ,C $\gamma$
	Ser <sup>51<math>\alpha</math></sup>	C $\beta$	vdw	Ala <sup>158</sup>	C $\beta$
		O $\gamma$	vdw	Gly <sup>162</sup>	C $\alpha$
		O $\gamma$	h-b	Glu <sup>166</sup>	O $\epsilon$ 1
CDR3 $\alpha$	Ser <sup>93<math>\alpha</math></sup> (V)	C $\beta$	vdw	P4-Lys	N $\zeta$
	Gly <sup>99<math>\alpha</math></sup> (J)	C=O	h-b	P4-Lys	N $\zeta$
	Phe <sup>100<math>\alpha</math></sup> (J)	C=O	polar	P4-Lys	N $\zeta$
		C $\alpha$	vdw	P4-Lys	N $\zeta$
		C $\beta$ ,C $\gamma$ ,C $\delta$	vdw	Gln <sup>65</sup>	C $\beta$ ,C $\gamma$
		C $\epsilon$	vdw	Arg <sup>62</sup>	C $\gamma$
	Ala <sup>101<math>\alpha</math></sup> (J)	C=O	h-b	P4-Lys	N $\zeta$
		NH	vdw	P4-Lys	N $\zeta$
CDR1 $\beta$	Thr <sup>26<math>\beta</math></sup>	C=O-wat	polar	Gln <sup>149</sup>	N $\epsilon$ -wat
	Asn <sup>28<math>\beta</math></sup>	C $\alpha$	vdw	Lys <sup>146</sup>	C $\epsilon$
		O $\delta$	polar	Gln <sup>149</sup>	N $\epsilon$
	His <sup>29<math>\beta</math></sup>	C $\alpha$	vdw	P6-Tyr	O $\eta$
		N $\delta$ 1	polar	P6-Tyr	O $\eta$
		C $\epsilon$ 1	vdw	Ala <sup>150</sup>	C $\beta$
	Asn <sup>30<math>\beta</math></sup>	NH	h-b	P6-Tyr	O $\eta$
		O $\delta$ 1	h-b	Lys <sup>146</sup>	N $\zeta$
		N $\delta$ 2	h-b	P7-Ser	O $\gamma$
	Asn <sup>31<math>\beta</math></sup>	N $\delta$ 2	vdw	P6-Tyr	C $\epsilon$
CDR2 $\beta$	Tyr <sup>50<math>\beta</math></sup>	C $\beta$	vdw	Val <sup>76</sup>	C $\gamma$
		C $\gamma$ ,C $\delta$	vdw	Ser <sup>73*</sup>	C $\beta$ ,C $\alpha$ ,C=O
		C $\gamma$ ,C $\delta$	vdw	Gln <sup>72</sup>	C=O,C $\alpha$ ,C $\beta$
	Ala <sup>52<math>\beta</math></sup>	C=O	h-b	Arg <sup>79</sup>	N $\eta$ 1
	Thr <sup>55<math>\beta</math></sup>	C=O	polar	Gln <sup>72</sup>	N $\epsilon$
	Glu <sup>56<math>\beta</math></sup>	O $\epsilon$	h-b	Gln <sup>72</sup>	N $\epsilon$
CDR3 $\beta$	Gly <sup>97<math>\beta</math></sup> (D)	C $\alpha$	vdw	Arg <sup>155*</sup>	C $\delta$ ,C $\zeta$ ,N $\eta$ 1
		C $\alpha$	vdw	P6-Tyr	C $\epsilon$ ,O $\eta$





TCR recognition repertoire and accommodating multiple peptide ligands. In antibodies, large CDR conformational changes, particularly in CDR-H3, have been documented upon antigen binding, particularly with peptides and small molecules (45). Analogous to the TCR, which does not undergo affinity maturation, germline antibodies have been seen to utilize conformational change as a means of compensating for nonoptimal complementarity to their antigen (46). However, the major conformational changes in the TCR are localized to the combining site and do not appear to have propagated through the molecule to the constant domains that presumably interact with the signal-transducing CD3 chains.

The H-2K<sup>b</sup>-dEV8 undergoes much less conformational adjustment in the binding interface than the TCR, but a large change has occurred in the positions of the α3-β<sub>2</sub>M domains relative to the α1α2 domains (Fig. 4B). The α3-β<sub>2</sub>M domains undergo a large torqueing in their pairing (15°) and a swiveling around Leu<sup>178</sup> (Fig. 4B) (43), which has been implicated as a pivot point for α3 movement in the HLA-A2-CD8<sub>αα</sub> complex (47). Whether these domain changes are the result of engagement of the TCR remains unclear.

**Comparison of 2C-H-2K<sup>b</sup>-dEV8 to A6-HLA-A2-Tax.** The most obvious differences between the two complexes are the extents to which the TCR β chains contact the pMHC and the TCR-MHC contacts used (16), given that the overall footprints are roughly similar. In striking contrast to 2C, the A6 TCR β chain CDRs 1 and 2

have essentially no contact with the pMHC surface (with the exception of one CDR1<sub>β</sub> interaction); the A6 CDR3<sub>β</sub> has a vast footprint covering the whole COOH-terminal half of the peptide (16, 30) (Fig. 4C). The difference in the β chain position is not solely due to the long CDR3<sub>β</sub> of A6, however. The pairing of the A6 TCR α and β chains deviates greatly from 2C (~11°) and is highly unusual compared with the V<sub>H</sub>-V<sub>L</sub> interfaces of antibodies (26, 40).

These two TCR-pMHC complexes suggest that the V<sub>α</sub> domains appear to be dominant in the orientation (but not necessarily in energetics) of the TCR-pMHC complex. This notion is supported by the relatively close superposition of the 2C V<sub>α</sub> with A6 V<sub>α</sub> in their respective pMHC complexes, and the fact that the A6 V<sub>β</sub> CDRs 1 and 2 do not contribute substantially to the interaction of that complex. There is an extremely close superposition of both CDRs 1 and 2 of the α chain and the corresponding residue positions 27<sub>α</sub> and 51<sub>α</sub>, which have been implicated by mutagenesis as being key in determining the class I or class II restriction of a TCR (32). In both complexes, Ser<sup>27α</sup> interacts with Glu<sup>58</sup> of the α1 helix, which is highly conserved in MHC heavy chains, and Ser<sup>51α</sup> contacts Ala<sup>158</sup> (in 2C this Ser<sup>51α</sup> also contacts Gly<sup>162</sup> and Glu<sup>166</sup>). Although the overall TCR V<sub>α</sub> domain incident angle with the pMHC surface is quite different, the tips of the CDRs 1<sub>α</sub> and 2<sub>α</sub> contacting the MHC helices fall in very similar positions.

An equally important difference in the two complexes is the TCR contact with, and respective positions of, the dEV8 and Tax

peptides. The A6 TCR has more extensive direct interactions with the Tax peptide, although the TCR-pMHC interface still exhibits poor shape complementarity and predominantly helical contact (16, 37). The closer abutment of the A6 TCR to the peptide is partially a result of the Tax peptide sitting higher in the MHC binding groove (16) than when dEV8 is bound to H-2K<sup>b</sup>. The more extensive A6 contact with Tax is consistent with this peptide's greater antigenicity (48) compared with the weakly agonistic dEV8 peptide in the 2C system. The accessibility of the Tax peptide epitope could be manifested in an energetic stabilization of the A6-HLA-A2-Tax complex, leading to a strong immune response. Thus, the strikingly different extents of peptide contact in the two complexes is potentially rationalized by the biological origins of these two different TCR-pMHC complexes.

## REFERENCES AND NOTES

1. H. Katz, T. Hamaoka, M. E. Dorf, B. Benacerraf, *Proc. Natl. Acad. Sci. U.S.A.* **70**, 2624 (1973); R. M. Zinkernagel and P. C. Doherty, *Nature* **248**, 701 (1974).
2. J. P. Allison *et al.*, *Immunol. Rev.* **81**, 145 (1984); S. C. Meuer, O. Acuto, T. Hercend, S. F. Schlossman, E. L. Reinherz, *Annu. Rev. Immunol.* **2**, 23 (1984); K. Haskins, J. Kappler, P. Marrack, *ibid.*, p. 51; A. R. Townsend *et al.*, *Cell* **44**, 959 (1986); Z. Dembic *et al.*, *Nature* **320**, 232 (1986); T. Saito and R. N. Germain, *ibid.* **329**, 256 (1987).
3. C. A. Janeway Jr., *Annu. Rev. Immunol.* **10**, 645 (1992).
4. C. Terhorst *et al.*, in *T Cell Receptors*, J. I. Bell, M. J. Owen, E. Simpson, Eds. (Oxford Univ. Press, New York, 1995), pp. 369-402.
5. K. Kuzushima, R. Sun, G. M. van Bleek, Z. Vegh, S. G. Nathanson, *J. Immunol.* **155**, 594 (1995); N. K. Nanda,

- K. K. Arzoo, H. M. Geysen, A. Sette, E. E. Sercarz, *J. Exp. Med.* **182**, 531 (1995); K. W. Wucherpfennig and J. L. Strominger, *Cell* **80**, 695 (1995); L. J. Ausubel, C. K. Kwan, A. Sette, V. Kuchroo, D. A. Hafter, *Proc. Natl. Acad. Sci. U.S.A.* **93**, 15317 (1996); G. J. Kersh and P. M. Allen, *J. Exp. Med.* **184**, 1259 (1996).
- M. D. Tallquist and L. R. Pease, *J. Immunol.* **155**, 2419 (1995); M. D. Tallquist, T. J. Yun, L. R. Pease, *J. Exp. Med.* **184**, 1017 (1996); M. D. Tallquist, A. J. Weaver, L. R. Pease, *J. Immunol.* **160**, 802 (1998).
- S. C. Jameson and M. J. Bevan, *Immunity* **2**, 1 (1995).
- G. J. Kersh and P. M. Allen, *Nature* **380**, 495 (1996); J. Madrenas and R. N. Germain, *Semin. Immunol.* **8**, 83 (1996).
- M. Vergelli et al., *J. Immunol.* **158**, 3746 (1997).
- S. C. Jameson, K. A. Hogquist, M. J. Bevan, *Annu. Rev. Immunol.* **13**, 93 (1995).
- L. A. Sherman and S. Chattopadhyay, *ibid.* **11**, 385 (1993).
- D. S. Lyons et al., *Immunity* **5**, 53 (1996); S. M. Alam et al., *Nature* **381**, 616 (1996); J. Madrenas, L. A. Chau, J. Smith, J. A. Bluestone, R. N. Germain, *J. Exp. Med.* **185**, 219 (1997).
- G. A. Bentley, G. Bouliot, K. Karjalainen, R. A. Mariuzza, *Science* **267**, 1984 (1995); B. A. Fields et al., *ibid.* **270**, 1821 (1995); D. Housset et al., *EMBO J.* **16**, 4205 (1997); J. H. Wang et al., *EMBO J.* **17**, 10 (1998).
- I. A. Wilson and K. C. Garcia, *Curr. Opin. Struct. Biol.* **7**, 839 (1997).
- K. C. Garcia et al., *Science* **274**, 209 (1996).
- D. N. Garboczi et al., *Nature* **384**, 134 (1996).
- M. M. Davis and P. J. Bjorkman, *ibid.* **334**, 395 (1988).
- R. N. Germain, *ibid.* **344**, 19 (1990).
- S. C. Hong et al., *Cell* **69**, 999 (1992).
- D. M. Kranz, D. H. Sherman, M. V. Sitkovsky, M. S. Pasternack, H. N. Eisen, *Proc. Natl. Acad. Sci. U.S.A.* **81**, 573 (1984).
- W. C. Sha et al., *Nature* **335**, 271 (1988); W. C. Sha et al., *ibid.* **336**, 73 (1988); J. K. Pullen, H. D. Hunt, R. M. Horton, L. R. Pease, *J. Immunol.* **143**, 1674 (1989); W. C. Sha et al., *Proc. Natl. Acad. Sci. U.S.A.* **87**, 6186 (1990).
- K. Uchida, T. J. Tsomides, H. N. Eisen, *Cell* **69**, 989 (1992).
- K. C. Garcia et al., *Proc. Natl. Acad. Sci. U.S.A.* **94**, 13838 (1997).
- Single-letter abbreviations for the amino acid residues are as follows: A, Ala; C, Cys; D, Asp; E, Glu; F, Phe; G, Gly; H, His; I, Ile; K, Lys; L, Leu; M, Met; N, Asn; P, Pro; Q, Gln; R, Arg; S, Ser; T, Thr; V, Val; W, Trp; and Y, Tyr.
- X-ray crystallographic programs and methods. (i) X-PLOR: A. T. Brünger, J. Kuriyan, M. Karplus, *Science* **235**, 458 (1987); A. T. Brünger, X-PLOR, Version 3.1: A System for X-ray and NMR (Yale Univ. Press, New Haven, CT, 1992). (ii)  $R_{\text{free}}$ : A. T. Brünger, *Nature* **355**, 472 (1992). (iii) Torsional dynamics: L. M. Rice and A. T. Brünger, *Proteins* **19**(4), 277 (1994). (iv) CCP4: Collaborative Computational Project No. 4, Daresbury, UK (1994); *Acta Cryst. D* **50**, 760 (1994). (v) O: T. A. Jones, J.-Y. Zou, S. W. Cowan, M. Kjeldgaard, *Acta Cryst. A* **47**, 110 (1991). (vi) SIGMA: R. J. Read, *ibid.* **42**, 140 (1986). (vii) AMoRe: J. Navaza, *ibid.* **50**, 157 (1994). (ix) DENZO and SCALEPACK: Z. Otwinowski, in *Data Collection and Processing*, L. Sawyer, N. Isaacs, S. Bailey, Eds. (SERC Daresbury Laboratory, Warrington, UK, 1993), p. 56. (viii) RAVE/MAMA: T. A. Jones, in *Molecular Replacement*, E. Dodson, Ed. (SERC Daresbury Laboratory, Warrington, UK, 1992), p. 91. (ix) PRO-CHECK: R. A. Laskowski, M. W. MacArthur, S. D. Moss, J. M. Thornton, *J. Appl. Cryst.* **26**, 283 (1993). (x) Rmsd's were calculated with PROFIT v.1.7 (A. C. R. Martin, SciTech Software, 1992–1996). (xi) Molecular surface areas buried by interaction were calculated with the program MS [M. L. Connolly, *J. Appl. Crystallog.* **16**, 439 (1983)] by using a 1.7 Å probe sphere, 10-point spot density, and standard atomic radii. (xii) AVS: C. Upson, *IEEE Comput. Graph. Appl.* **9**, 30 (1989). (xiii) PQMS: M. L. Connolly, *J. Mol. Graph.* **11**, 139 (1993). (xiv) "Shake" omit maps: D. E. McRee, *Practical Protein Crystallography* (Academic Press, New York, 1993). (xv) Resolution estimate: G. J. Kleywegt and T. A. Jones, *Acta Cryst. D* **52**, 826 (1996).
- The two 2C–H-2K<sup>b</sup>–dEV8 complexes in the asymmetric unit are highly similar (0.3 Å rmsd). Only one of the two complexes (molecule 1) has been used for the analysis here. When the 2C TCR in the complex is compared with the unliganded 2C, the individual  $\alpha$  and  $\beta$  chains superimpose with rmsd's of 1.2 and 0.7 Å, respectively, over all  $\alpha$  carbons. The pairing of the  $V_{\alpha}$  and  $V_{\beta}$  domains has slightly changed by 3.5° in the complex, the elbow angle relating the pseudo twofold symmetry of the  $V_{\alpha}$  to the  $C_{\alpha}C_{\beta}$  has remained constant at 148.6°, and the buried surface areas between  $V_{\alpha}$ – $V_{\beta}$  (~1300 Å<sup>2</sup>) and  $C_{\alpha}$ – $C_{\beta}$  (~2350 Å<sup>2</sup>) are also similar. A pairwise comparison of A6 against the Fab structural database indicates that the A6  $V_{\alpha}$ – $V_{\beta}$  pairing differs from known Fab  $V_{\alpha}$ – $V_{\beta}$  pairings by between 16° and 28°, which is beyond the normal range of pairing differences seen among antibodies. Pairwise comparison of the 2C TCR in the complex with A6 indicates that an 11° rotation and 2.5 Å translation are required to bring the  $V_{\beta}$  domains into alignment after first superimposing the  $V_{\alpha}$  domains. Methods for pairwise comparisons, superpositions, and measurements of interdomain angles in TCRs and their comparison to antibodies have been described (15).
- The noncrystallographic symmetry relating the two molecules in the asymmetric unit of this TCR–pMHC complex crystal is of questionable biological relevance. The two complexes are oriented in opposite directions, which would be difficult to achieve in vivo when considering the polarity of the interaction surface of the T cell when in contact with an antigen-presenting cell. However, the situation in the crystal cannot be extrapolated directly to the in vivo environment, where higher order oligomers are an integral step in the TCR signaling complex [R. N. Germain, *Curr. Biol.* **7**, R640 (1997)].
- J. Brown et al., *Nature* **364**, 33 (1993); B. A. Fields and R. A. Mariuzza, *Immunol. Today* **7**, 330 (1996).
- D. H. Fremont, M. Matsumura, E. A. Stura, P. A. Peterson, I. A. Wilson, *Science* **257**, 919 (1992).
- The total buried surface area in the interface of the A6–HLA-A2–Tax complex (16) is ~1800 Å<sup>2</sup> (895 Å<sup>2</sup> for the A6 TCR and 912 Å<sup>2</sup> for HLA-A2–Tax). When divided by CDR the numbers are as follows: CDR1 $\alpha$ , 225 Å<sup>2</sup>; CDR2 $\alpha$ , 90 Å<sup>2</sup>; HV4 $\alpha$ , 42 Å<sup>2</sup>; CDR3 $\alpha$ , 216 Å<sup>2</sup>; CDR1 $\beta$ , 17 Å<sup>2</sup>; and CDR3 $\beta$ , 290 Å<sup>2</sup>. These values were calculated with MS (25).
- S. P. Clark, B. Arden, D. Kabelitz, T. W. Mak, *Immunogenetics* **42**, 531 (1995).
- B.-C. Sim, L. Zerva, M. I. Greene, N. R. J. Gascoigne, *Science* **273**, 963 (1996).
- J. Klein, *Natural History of the Major Histocompatibility Complex* (Wiley, New York, 1996).
- K. Matsui et al., *Science* **254**, 1788 (1991).
- J. Speir et al., submitted.
- J. Jorgensen, P. Reay, E. Ehrlich, M. Davis, *Annu. Rev. Immunol.* **10**, 835 (1992).
- Calculation of a general shape complementarity index for protein-protein interfaces has been approximated [M. C. Lawrence and P. M. Colman, *J. Mol. Biol.* **234**, 946 (1993)]. Application of this algorithm to the 2C–H-2K<sup>b</sup>–dEV8 interface gives a value of 0.45. The value calculated for A6–HLA-A2–Tax is 0.47. For comparison, antibody-antigen complexes (0.66 to 0.68) and protein oligomeric interfaces (0.68 to 0.75) give values indicating better shape complementarity. The weak interaction of a crystal lattice contact gives a value of 0.35. Thus, according to this measurement, the shape complementarity of the TCR–pMHC interfaces are both quite poor.
- K. Uchida, K. H. Wiesmuller, S. Kienle, G. Jung, P. Walden, *Immunology* **157**, 670 (1996).
- T. J. Pawlowski, M. D. Singleton, D. Y. Loh, R. Berg, U. D. Staerz, *Eur. J. Immunol.* **26**, 85 (1996); L. Ignatowicz, J. Kappler, P. Marrack, *Cell* **84**, 521 (1996); M. Bevan, *Immunity* **7**, 175 (1997).
- I. A. Wilson and R. L. Stanfield, *Curr. Opin. Struct. Biol.* **4**, 857 (1994).
- S. C. Cose, J. M. Kelly, F. R. Carbone, *J. Virol.* **69**, 5849 (1995).
- J. Nikolic-Zugic and M. J. Bevan, *Nature* **344**, 65 (1990); D. Brandle et al., *Eur. J. Immunol.* **21**, 2195 (1991).
- The  $\alpha 1$  and  $\alpha 2$  helices of free and bound pMHC superimpose closely (0.72 Å rmsd between  $C_{\alpha}$  atoms) and the dEV8 octamer peptide conformation is highly similar to other H-2K<sup>b</sup>–bound octamer peptides (0.96 Å rmsd). However, in the complex, the dEV8 peptide has undergone a main chain shift of ~1.5 Å at the P5 and P6 positions. This shift can possibly be explained by the presence of a water molecule in the unliganded H-2K<sup>b</sup>–dEV8, which forms a hydrogen-bond bridge between the highly polymorphic Glu<sup>152</sup> and the P6 backbone amide. In the TCR complex, this water does not appear to be present, because the corresponding Glu<sup>152</sup> hydrogen bonds directly to the P6 backbone amide. The different conformation of the Tyr<sup>P6</sup>  $\chi_1$  dihedral angle in the unliganded H-2K<sup>b</sup>–dEV8 is due, in part, to a crystal contact in which the Tyr<sup>P6</sup> hydrogen bonds to a neighboring symmetry-related MHC molecule. When the  $\alpha 1\alpha 2$  domains are optimally aligned, the  $\alpha 3$  and  $\beta_2$  M superimpose with rmsd's of 2.5 and 4.3 Å, respectively (over all backbone atoms).
- T. N. Bhat, G. A. Bentley, T. O. Fischmann, G. Bouliot, R. J. Poljak, *Nature* **347**, 483 (1990).
- R. L. Stanfield, M. Takimoto-Kamimura, J. M. Rini, A. T. Profy, I. A. Wilson, *Structure* **1**, 83 (1993); J. N. Herron et al., *Proteins* **11**, 159 (1991); J. M. Rini, U. Schulze-Gahmen, I. A. Wilson, *Science* **255**, 959 (1992).
- G. J. Wedemayer, P. A. Patten, L. H. Wang, P. G. Schultz, R. C. Stevens, *Science* **276**, 1665 (1997).
- G. F. Gao et al., *Nature* **387**, 630 (1997).
- U. Utz, D. Banks, S. Jacobson, W. E. Biddison, *J. Virol.* **70**, 843 (1996).
- D. H. Fremont, E. A. Stura, M. Matsumura, P. A. Peterson, I. A. Wilson, *Proc. Natl. Acad. Sci. U.S.A.* **92**, 2479 (1995).
- Crystals of H-2K<sup>b</sup> in complex with the dEV8 peptide were obtained from 2.0 M phosphate at pH 6.5 containing 1.0% methylpentanediol by using the sitting drop vapor diffusion method. The crystals were isomorphous to those previously reported for H-2K<sup>b</sup>–SEV-9 and –VSV-8 peptide complexes (29). A diffraction data set to 2.3 Å was collected at –180°C (Oxford Cryosystems) on a Mar imaging plate mounted on a Siemens x-ray generator operating at 40 kV and 50 mA with Supper double-focusing long mirrors. Data were processed with DENZO and SCALEPACK (25). The refined model of H-2K<sup>b</sup>–VSV (29) was used for the refinement after the peptide atoms were removed. Refinement of the individual  $\alpha 1$ ,  $\alpha 2$ ,  $\alpha 3$ , and  $\beta_2$  M domains was carried out in X-PLOR (25).  $R_{\text{free}}$  cross-validation based on 1217 reflections (5%) was used throughout the refinement (25). Continuous density for the peptide was apparent in the binding groove after simulated annealing. Refinement proceeded by alternating positional and individual temperature factor refinement with manual rebuilding in  $\sigma_A$ -weighted (25)  $2F_o - F_c$  and  $F_o - F_c$  maps with the program O (25). The final model contains all protein residues as well as four N-linked carbohydrate moieties and 184 ordered water molecules. Scattering of the bulk solvent was accounted for by using a flat model.
- Iterative contacts were evaluated both on distance and geometrical considerations. Van der Waals (<4.5 Å) and hydrogen-bond (<3.5 Å) interactions were calculated with the program CONTACTSYM [S. Sheriff, W. A. Hendrickson, J. L. Smith, *J. Mol. Biol.* **197**, 273 (1987)]. The designation "polar" was assigned to hydrogen-bond interactions that were within proper hydrogen-bonding distance but whose geometry deviates from ideality [I. K. McDonald and J. M. Thornton, *ibid.* **238**, 777 (1994)], possibly because of the atomic error inherent in 3.0 Å x-ray data.
- We thank F. Carbone, D. H. Kranz, and M. Tallquist for discussions and sharing unpublished results; M. Pique for production of figures; N. Gascoigne and J. Johnson for discussions; D. C. Wiley for coordinates of the A6–HLA-A2–Tax structure; and R. Stefanko for technical assistance. Supported by NIH R01 CA58896 (I.A.W.), AI42266 (I.A.W.), AI42267 (L.T.), and the R. W. Johnson Pharmaceutical Research Institute (L.T.). The coordinates for 2C–H-2K<sup>b</sup>–dEV8 have been deposited in the Protein Data Bank (PDB) (accession number 2CKB).

24 October 1997; accepted 7 January 1998